Int. J. Electrochem. Sci., 6 **(2011)** 2943 - 2954

International Journal of
ELECTROCHEMICAL
SCIENCE
www.electrochemsci.org

Solid-State Thermolysis Preparation of Co_3O_4 Nano/Micro Superstructures From Metal-Organic Framework for Supercapacitors

Fang Zhang, Liang Hao, Luojiang Zhang, Xiaogang Zhang[*]

College of Material Science & Technology, Nanjing University of Aeronautics and Astronautics, Nanjing 210016, China
[*]E-mail: azhangxg@163.com

Received: 4 May 2011 / *Accepted:* 4 June 2011 / *Published:* 1 July 2011

We describe here a novel strategy for the preparation of Co_3O_4 nano/micro superstructures from a cobalt ion-based metal-organic framework (MOF). First, cobalt ion-based coordination polymer with metal-organic framework was synthesized through solvothermal method by using *p*-benzenedicarboxylic acid (*p*-H_2BDC) as ligand. Second, porous Co_3O_4 nano/micro superstructures were prepared from solid-state annealing of MOF precursor at 450 ℃ for 2 h. The resulting superstructures were assembled by porous microsheet building blocks, which primarily composed of uniform nanoparticles. When used as electrode material of supercapacitors, the as-prepared porous Co_3O_4 superstructures exhibited a specific capacitance of 208 $F \cdot g^{-1}$ at the current density of 1 $A \cdot g^{-1}$ and a specific capacitance retention of *ca.* 97% after 1000 continuous charge-discharge cycles in 6.0 M aqueous KOH solution (vs. SCE), suggesting their potential applications for supercapacitors.

Keywords: Co_3O_4, superstructures, metal-organic framework, supercapacitors

1. INTRODUCTION

Recent years electrochemical capacitors, also known as supercapacitors, have drawn much attention because they combined the advantages of both conventional dielectric capacitors and rechargeable batteries, i.e., the delivery of high-power in a short time and the ability to store high energy, which make them potentially the most important next generation energy devices [1-3]. As the core component of supercapacitors, electrode material plays an important role in determining the performance of electrochemical capacitors. Therefore, rapid development of new material with high performance is essential. Nanostructured materials are currently of high interest for supercapacitors benefit from their high surface area and novel size effect [4-7]. Nevertheless, the disadvantages of

nanoscale electrode materials, such as low thermodynamic stability and high activity towards surface reaction, were unfavorable for their practical applications [8]. It has been well established that electrode material self-assembled with nano/micro hierarchical structures are one of the best systems in the field of supercapacitors [9-10]. The nano/micro hierarchical structures assembled from nanoparticles, combined with the advantages of both nanoparticles and micro- or submicrometer-sized assemblies, are expected to display high performance for supercapacitors.

Cobalt oxides, in particular spinel Co_3O_4, have been the subject of intense interest due to their wide-range applications in catalysts [11-13], magnetic material [14-15], sensors [16-17] and electrochemistry [18-19]. The past few years, considerable effort has been devoted to develop various methods to synthesize Co_3O_4 micro- and nanostructures for supercapacitors. For instance, needle-like Co_3O_4 nanorods were synthesized by a polymer-assisted hydrothermal method and sequential heat treatment [20]; mesoporous Co_3O_4 microspheres were fabricated through a hard template route [21]; Co_3O_4 nanoplates were prepared by a facile binary-solution route and sequential thermal decomposition [22].

Recently, some coordination polymers with metal-organic framework have been utilized to generate metal oxides micro- and nanostructure with regular shape. For instance, Xie et al. prepared γ-MnO_2 [23] nanowires and ZnO nanorods [24] via a solution-based thermolysis procedure by using right coordination polymer as precursors. From the crystallography viewpoint and growth mechanism, it may be an effective and reasonable method. But the selection of precursor is crucial to control the morphology and size of metal oxides. It is highly desirable to understand the formation mechanism of metal oxides micro- and nanostructure generated from coordination polymer with various types of metal-organic framework under different condition.

For its strong chelating ability and diverse bridging tendency, coordination polymers based on *p*-benzendicarboxylic acid (*p*-H_2BDC) has been studied extensively, much effort has been devoted to design and synthesis of metal-organic framework with permanent porosity [25-26]. In the present work, we introduce a simple calcination procedure to prepare porous Co_3O_4 nano/micro superstructures from the cobalt-*p*-benzendicarboxylic acid (Co-*p*-BDC) coordination polymer. Electrochemical measurements demonstrate that the as-prepared Co_3O_4 nano/micro superstructures can offer a large specific capacitance and a high electrochemical stability. The effects of annealing temperature on the capacity of porous Co_3O_4 nano/micro superstructures also have been discussed.

2. EXPERIMENTAL

2.1. Synthesis of cobalt ion-based coordination polymer and preparation of Co_3O_4 nano/micro superstructures

All chemicals were of analytical grade and used as received without further purification. In a typical procedure, $CoCl_2 \cdot 6H_2O$ (0.349 g) and *p*-benzenedicarboxylic acid (*p*-H_2BDC) (0.166 g) were added into distilled water and N, N-dimethylformamide (DMF) (10 mL/5 mL) with vigorous stirring at room temperature for 30 mins. The mixture was then transformed into a Teflon-lined stainless steel

autoclave, which was heated gradually to 180 ℃ and maintained at this temperature for 12 h followed by cooling down to room temperature at a cooling rate of 2 ℃/h. The pink-colored product was collected by centrifugation and washed with distilled water for several times, before drying at 40 ℃ in an oven. Solid-state annealing of coordination polymer was performed in a tube furnace with both-ends opened to air at temperature up to 450 ℃ for 2h with a heating rate of 5 ℃·min^{-1}. Similarly, annealing of coordination polymer at 550 and 650 ℃ followed the same condition.

2.2. Characterization of cobalt ion-based coordination polymer and Co_3O_4 nano/micro superstructures

Fourier transform infrared (FT-IR) spectra of *p*-H_2BDC and Co-BDC coordination complex were recorded from KBr pellets in the range of 400 - 4000 cm^{-1} on a Nicolet 5DX spectrometer. Element analysis of Co-BDC coordination complex was done by Perkin-Elmer 240 analyzer. Thermogravimetry/differential scanning calorimetry (TG-DSC) of Co-BDC coordination complex was performed on thermogravimetry analyzer (NETZSCH STA 409) with a heating rate of 20 ℃·min^{-1} and an air flow rate of 20 mL·min^{-1}. X-ray powder diffraction (XRD) pattern of thermal decomposed product was acquired on a Bruker D8 powder X-ray diffractometer with graphite monochromatized Cu*Ka* radiation (λ = 1.5406 Å). SEM images and EDX spectrum of the Co_3O_4 nano/micro structures were taken with a field emission scanning electron microscope (LEO 1530 VP). TEM images were taken on a transmission electron microscope (FEI Tecnai-G2) with an accelerating voltage of 200 kV. The BET measurements were determined by using Micromeritics ASAP2010 surface area analyzer.

2.3. Preparation and electrochemical measurements of Co_3O_4 electrode

All electrochemical measurements were performed on a CHI660 electrochemical workstation (Shanghai Chenhua Co. Ltd. China) in a three-electrode system with Pt foil as the counter electrode and a standard calomel electrode (SCE) as the reference electrode. The working electrode was prepared by mixing the active material (Co_3O_4, 80 wt%), acetylene black (15 wt%) and polytetrafluoroethylene (5 wt%). The mixture was then pressed onto a nickel grid (1 cm^2) and dried at 50 ℃. All electrodes were tested in a 6.0 M KOH aqueous electrolyte and all electrochemical measurements were carried out at room temperature.

3. RESULTS AND DISCUSSION

3.1. Characterization of cobalt ion-based coordination polymer and its decomposed product

FT-IR spectrum was employed to reveal the composition of the pink-colored product. For easy to compare, we recorded the spectra of *p*-H_2BDC ligand and Co-BDC coordination complex, the results were shown in Fig. 1. The FT-IR spectrum of aromatic carboxylic acid has been studied extensively and every absorption peak was assigned to corresponding vibration [27]. As shown in Fig.

1a, the characterization peaks at 1715 and 1411 cm^{-1} were attributed to the υ(C=O) and δ(O-H) stretching vibrations of carboxylic acid.

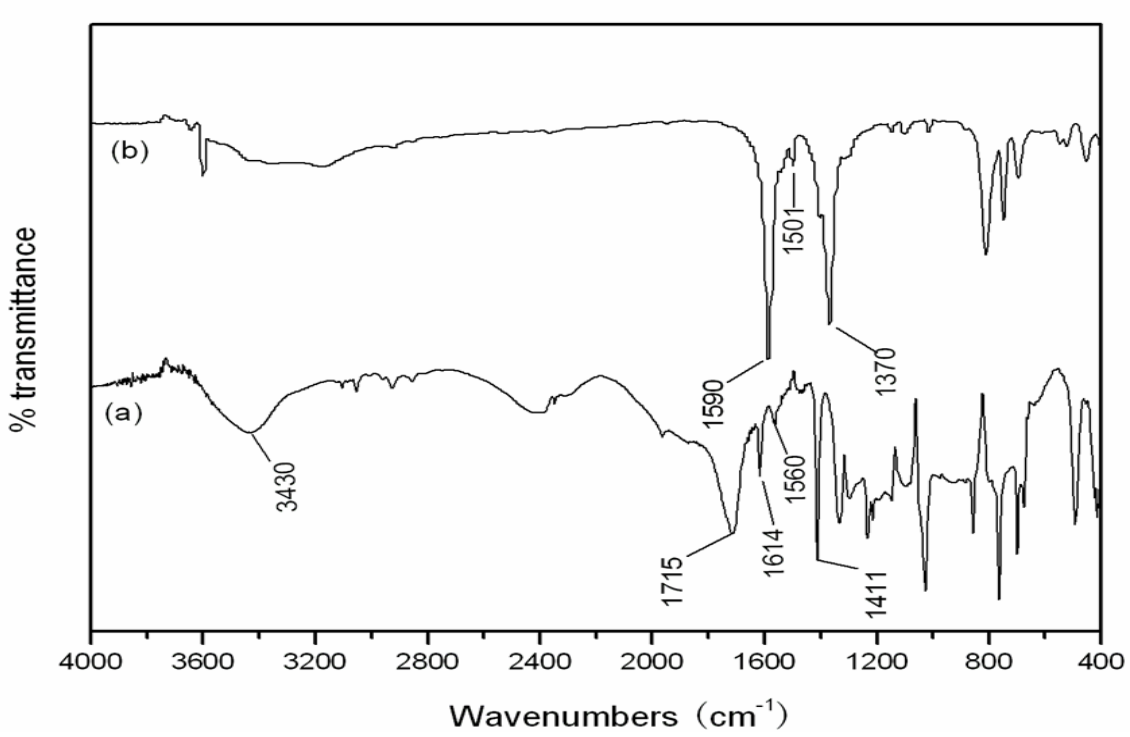

Figure 1. FT-IR spectra of (a) ligand *p*-H_2BDC and (b) as-synthesized cobalt ion-based coordination polymer

Two distinct absorption peaks at 1560 and 1614 cm^{-1} were attributed to the υ(C=C) stretch of benzene ring (Fig. 1a). By contrast with Fig. 1a, the characterization peak of C=O at 1715 cm^{-1} does not appear in the Fig. 1b, which indicates the coordination of carboxyl group to Co. The strong bands at 1590 and 1370 cm^{-1} were assigned to the asymmetric and symmetric stretching modes of coordinated (COO) group, respectively. Adsorptions due to the asymmetric and symmetric stretching of the coordinated COO groups in the 1610-1570 and 1390-1370 regions indicate that the BDC-Co complex have polymeric structures [28]. The weak band at 1501 cm^{-1} is the vibration of benzene ring υ(C=C). It is to note that broad band centered at 3430 cm^{-1} from H_2O of hydration does not appear in the Fig. 1b, which implies the absence of coordinated and free solvent H_2O molecules in the complex. The wavenumber separation ($\Delta\upsilon$) between $\upsilon_{as}(COO^-)$ and $\upsilon_s(COO^-)$ can be used to indentify the coordinate modes of carboxylic group to metal ion. The separation between asymmetric and symmetric stretching of COO^- anion is 220 cm^{-1}, which is greater than 200 cm^{-1}, indicating that the COO^- of *p*-BDC coordinated to Co in a monodentate mode.

The thermal stability of the as-synthesized BDC-Co coordination complex has been investigated by TG-DSC method. Fig. 2 shows the TG-DSC curves recorded from room temperature to 600 ℃. It is found that only one abrupt weight loss of 37.34% was observed from the temperature of 363 to 365 ℃, which is due to the decomposition of coordination polymer. Accordingly, the DSC

pattern shows an obvious exothermic peak for the decomposition and oxidation of coordination polymer to Co_3O_4. It is to note that no weight loss or endothermic peak were observed below 363 ℃, indicating the absence of coordinated or crystallized H_2O molecules in the coordination complex, which is in agreement with the IR result.

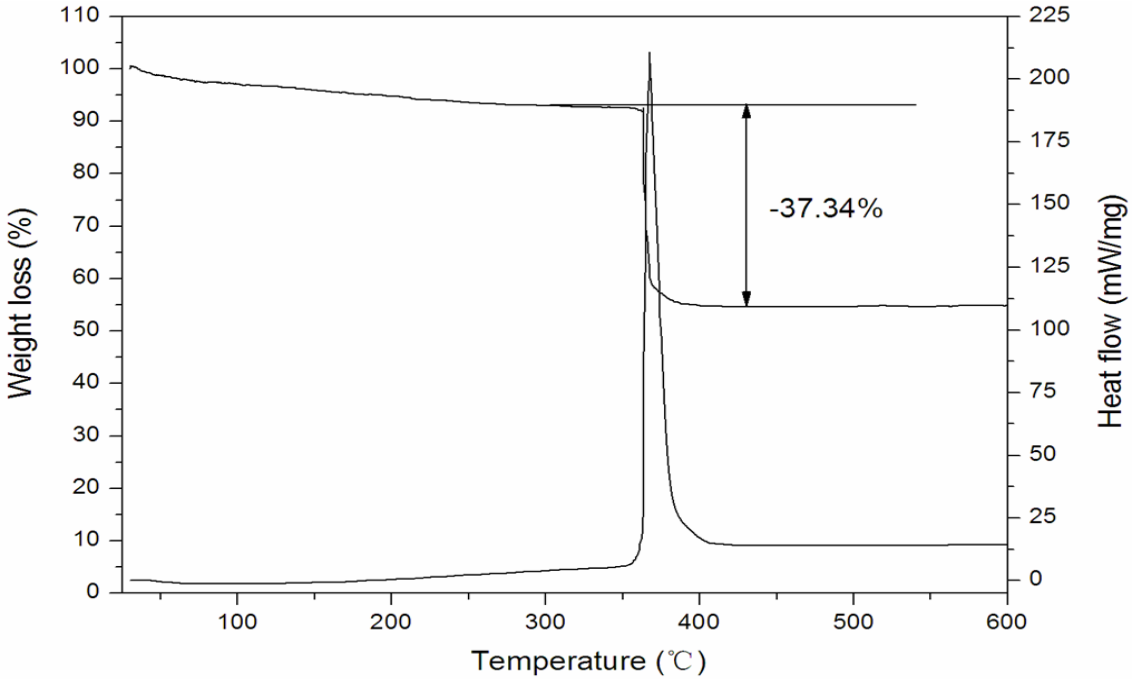

Figure 2. TG-DSC curves of as-synthesized cobalt ion-based coordination polymer

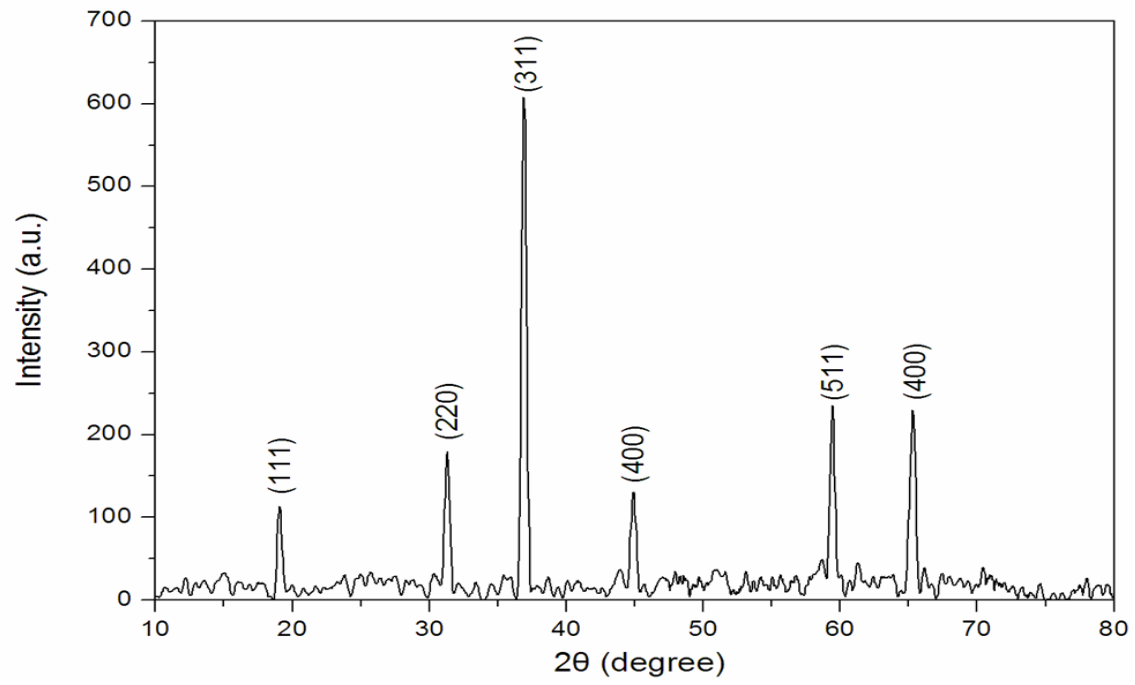

Figure 3. XRD pattern of thermal decomposed product at 450 ℃

On the basis of FT-IR, TG-DSC analysis and electrical neutrality supposition, we proposed that the probable molecular formula for the as-synthesized coordination complex is $[Co(BDC)_2H_2]_n$. Because the weight loss converted into Co_3O_4 based on the proposed molecular formula is 38%, which is very close to the value of measurement (37.34%). To confirm the supposition, the composition of the as-synthesized BDC-Co coordination complex was further examined by element analysis. EA(%) result calcd: C, 42.25; O, 37.52; Co, 17.28; H, 2.95; Found: C, 42.2; O, 37.6; Co, 17.6; H, 2.6. The determined EA(%) matched well with the calculated value from the formula of $[Co(BDC)_2H_2]_n$. Thus, the proposed molecular formula is reasonable.

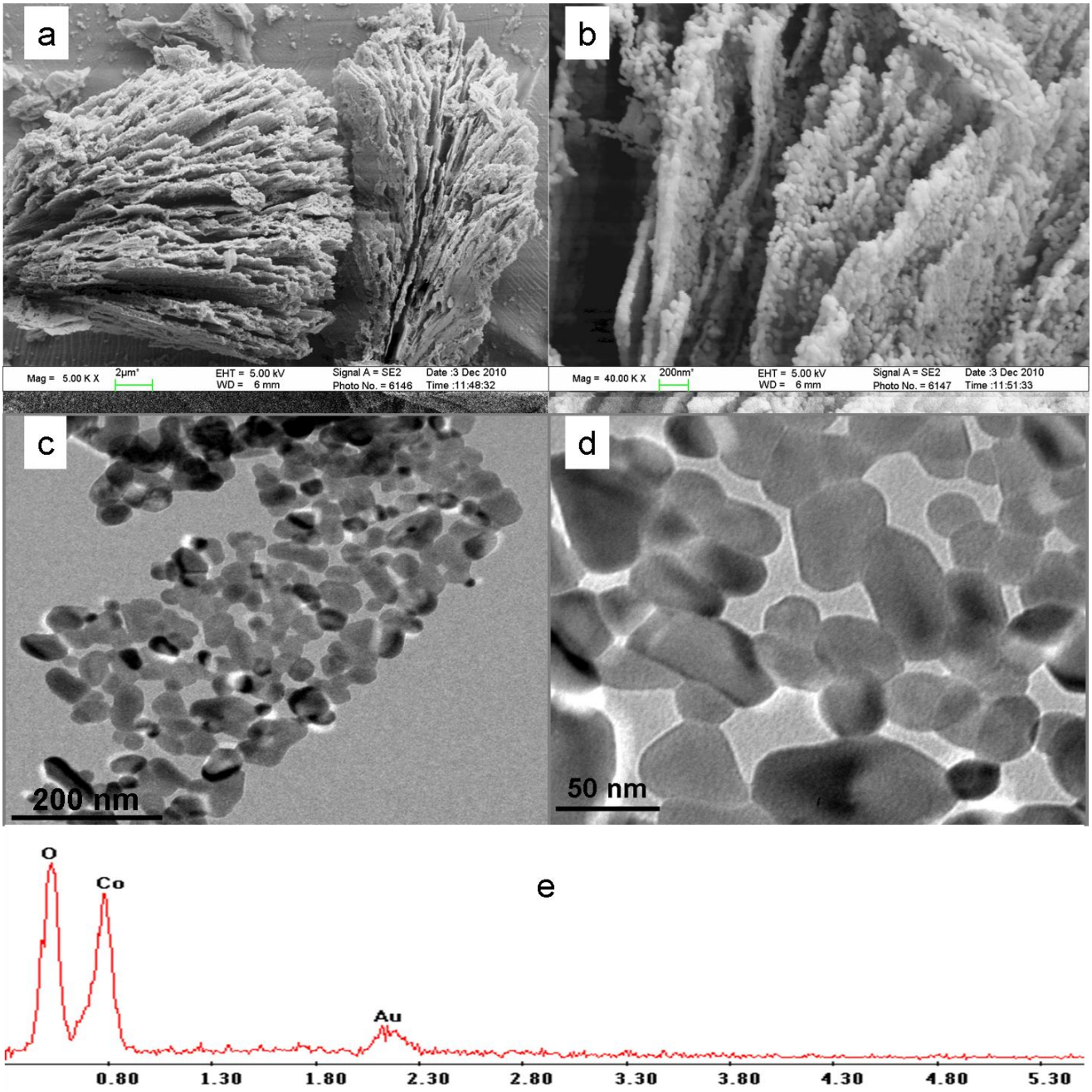

Figure 4. Typical FESEM images (a, b) and TEM images of Co_3O_4 nano/micro superstructures, (e) EDX spectrum obtained from Co_3O_4 nano/micro superstructures

According to the TG-DSC results, the heat treatment temperature of the *p*-BDC-Co coordination complex to Co_3O_4 was set at 450 ℃ to ensure the complete decomposition. The crystalline structure and phase purity of thermal decomposed product were examined by XRD pattern, the result was shown in Fig. 3. All the diffraction peaks in the Fig. 3 can be indexed to cubic phase Co_3O_4 (Lattice: face-centered; S.G.: *Fd3m* (227); Cell parameters: *a* = 8.0837 Å; JCPDS card no. 42-1467). No characterization peaks from other impurities were observed, indicating the high purity of decomposed product.

The morphology of the decomposed product was investigated by FESEM and TEM, respectively. The panoramic view in Figure 4a shows that the Co_3O_4 product consists of 3D superstructures, which actually assembled from hundreds of microscale two-dimensional sheets. The detailed morphology of Co_3O_4 superstructures is supported by the high-magnification image shown in Figure 4b, which reveals that these microscale sheets are densely composed of many uniform nanoparticles with an estimated mean size of *ca.* 30 nm. Furthermore, it can be clearly observed from the images that the accumulation of particles makes the microsheet form a great deal of pores between particles, which identified carefully in the nanosized scale. From TEM images (Fig. 4c and 4d), further information about the superstructures can be obtained. Fig. 4c clearly presents the projected shape of one microplate from Co_3O_4 superstructures, which are seen to be assembled by a large number of nanoparticles, consistent with the FESEM results. Additionally, the TEM image further demonstrated the porous nature of microsheets. A high-magnification image shown in Fig. 4b confirms the uniform size (*ca.* < 50 nm) of nanoparticles and the nanoscale pore size.

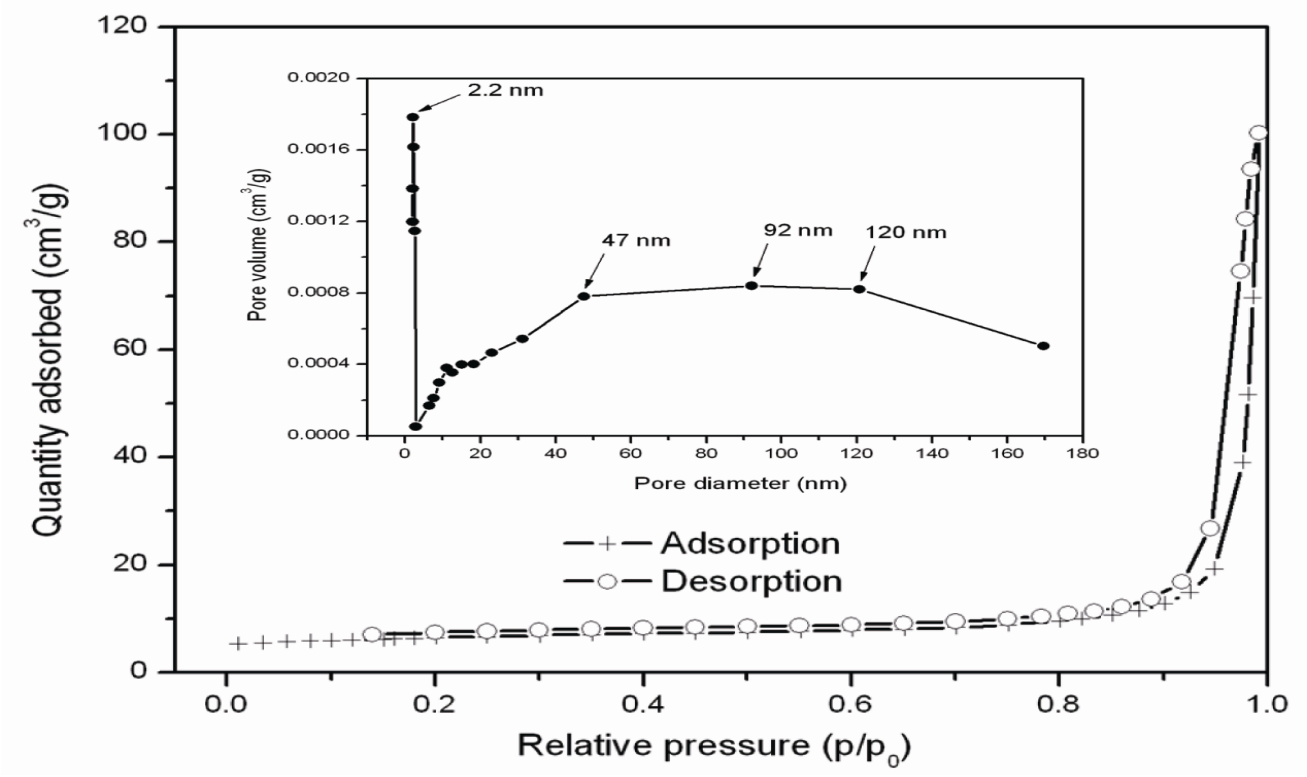

Figure 5. Nitrogen adsorption-desorption isotherms of the Co_3O_4 nano/micro superstructures measured at standard temperature and pressure (inset is the corresponding BJH pore size distribution plot)

An analysis by energy-dispersive X-ray (EDX) spectroscopy in Figure 4e demonstrates that the crystal is composed of Co and O (Au came from the sprinkled Au for SEM examination of the sample), furthermore atomic% confirms the right chemical formula of Co_3O_4.

To investigate the specific surface areas and the porous nature of the Co_3O_4 nano/micro superstructures, Brunauer-Emmett-Teller (BET) gas-sorption measurements were performed. Nitrogen adsorption-desorption isotherms of these nano/micro superstructures are shown in Figure 5, and the inset illustrates the corresponding Barrett-Joyner-Halenda (BJH) pore size distribution plot. The isotherms can be categorized as type of IV according to IUPAC classifications. The sharp increase in the uptake of N_2 at higher relative pressure (p/p_0>0.9) demonstrates the existence of macropores in the samples which due to the interparticle space. Furthermore, the uptake of N_2 in the macropore region is significantly for the sample, suggesting the presence of higher fraction of macropores. The BJH pore size distribution calculated from the adsorption curve revealed the presence of multimodal and hierarchical porosity: mesopores together with macropores. It can be observed from the plot that the pore size of great than 50 nm is relatively less intense. Therefore, the contribution of macropore volume to the total pore volume is comparatively less and the total porosity in the sample is mostly due to mesopores. The detailed textural properties of the Co_3O_4 nano/micro superstructure are quantitatively shown as follows: the BET specific surface area is 21.5 $cm^2 \cdot g^{-1}$, the pore volume is 0.16 $cm^3 \cdot g^{-1}$ and the average pore size is 28.8 nm. Such hierarchical porosity of Co_3O_4 nano/micro superstructures can facilitate electrolyte impregnating into particles and ensure that there are enough electrolyte ions to rapid contact the much larger surfaces of the electroactive Co_3O_4 materials. This is significant for supercapacitor electrode materials given a high-rate charge-discharge ability.

3.2. Electrochemical properties of Co_3O_4 nano/micro superstructures

To examine the effect of unique nano/micro superstructures to the electrochemical properties of Co_3O_4 electrode, the performance of the as-prepared Co_3O_4 nano/micro superstructures for supercapacitor was studied by cyclic voltammetry (CV), galvanostatic charge-discharge and cycling life measurements. Fig. 6a shows the CV curve of prepared Co_3O_4 nano/micro superstructures at a scan rate of 5 $mV \cdot s^{-1}$ within the potential range of 0.00 to 0.35 V (v. SCE). Two well-defined peaks were observed in the curve: the anode peak of P1(centered at 0.21 V) and cathodic peak of P2 (centered at 0.12 V). In addition, two weak peaks labeled as P3 and P4 in the potential range of 0.25-0.30 V also appeared in the same CV curve. In terms of previous literatures [29], these two pairs of peaks stand for the following two redox processes:

$$Co_3O_4 + OH^- + H_2O \leftrightarrow 3CoOOH + e^- \quad (1)$$

$$CoOOH + OH^- \leftrightarrow CoO_2 + H_2O + e^- \quad (2)$$

Clearly, the two pair redox peaks are responsible for the Faradaic pseudocapacitive property of Co_3O_4 electrode.

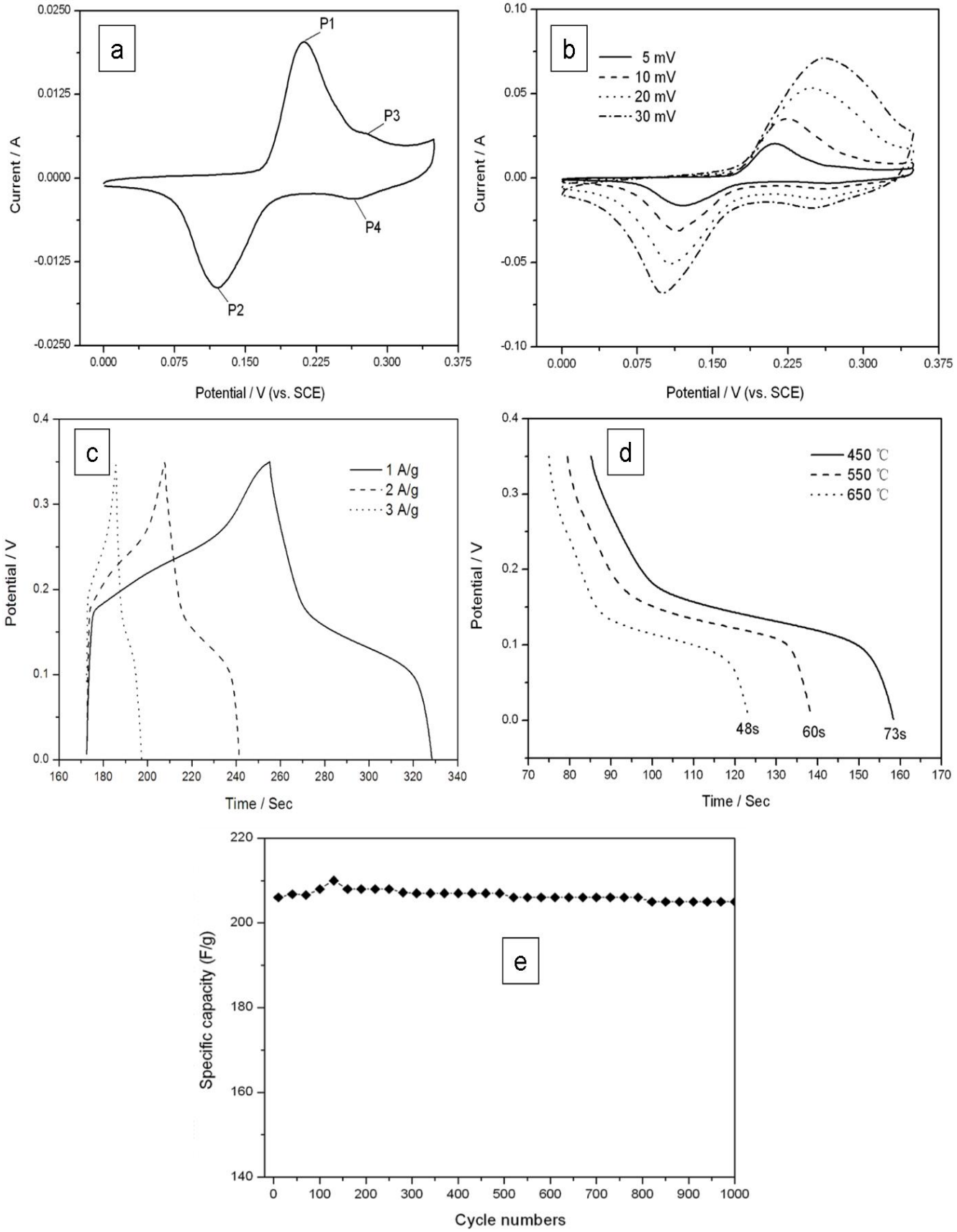

Figure 6. (a) CV curve at the scan rate of 5 $mV \cdot s^{-1}$, (b) CV curves at various scan rates, (c) CP plots at different current densities, (d) Discharge curves at different annealing temperature, and (e) cycle number of the as-prepared Co_3O_4 nano/micro superstructures

The CV curves shown in Fig. 6b are for the Co_3O_4 nano/micro superstructures at various scan rates relative to the first scan rate. It can be seen that the CV curves with good symmetry are independent of scan rate, indicating a stable reversibility of the redox reaction. The capacitance of Co_3O_4 electrode at various scan rates can be calculated from the following equation:

$$SC = \frac{q}{mv} = \frac{1}{0.35mv}\int_{0.35}^{0} I(V)dV \qquad (3)$$

The specific capacitance value of Co_3O_4 electrode at a low scan rate of 5 $mV \cdot s^{-1}$ is 210 $F \cdot g^{-1}$. Impressively, the specific capacitance value still retains 179 $F \cdot g^{-1}$ at a high scan rate of 30 $mV \cdot s^{-1}$. As is known, with the increase of scan rate, the diffusion of OH^- is much slower, and the ions only can reach the outer surface of the Co_3O_4 materials. Therefore, the effective utilization of the electroactive material has been greatly limited, leading to the decrease of specific capacitance [30-31]. In the present Co_3O_4 nano/micro superstructures, the hierarchical porosity made up of mesopores and macropores can supply enough electrolyte ions to rapidly contact the much larger surface and reduce the diffusion lengths, which in turn ensuring better utilization of the electroactive Co_3O_4 materials at a high scan rate.

To acquire more information for the supercapacitive performance of as-prepared Co_3O_4 electrode, galvanostatic charge-discharge measurement was performed in the potential range of 0 - 0.35 V (vs. SCE). Fig. 6c shows the charge-discharge curve of Co_3O_4 electrode at the current density of 1, 2 and 3 $A \cdot g^{-1}$. As it can be found, the discharge curve can be divided into two parts: a linear variation of potential versus on time (0 to 0.1 V) parallel to vertical axis which indicates a pure douber-layer capacitance behavior from the charge separation at the electrode/electrolyte interface. By contrast, a sloped variation of potential versus on time (0.1 to 0.35 V) caused by electrochemical adsorption/desorption or a redox reaction, indicates the typical pseudocapacitive behavior [32-33]. The specific capacitance of the electrode at different current densities can be calculated by using $C = It/\Delta Vm$, in which I is the discharge current, t is the total discharge time, ΔV is the potential drop during discharge, and m is the mass of Co_3O_4 within the composite electrodes. The specific capacitance value of Co_3O_4 nano/micro structures electrode are 208, 194, 102 $F \cdot g^{-1}$ at the current density of 1, 2, 3 $A \cdot g^{-1}$, respectively. These results demonstrate that the Co_3O_4 nano/micro superstructure is a better candidate for supercapacitor electrode compared with Co_3O_4 nanosheets [22] (92 $F \cdot g^{-1}$ at the current density of 5 $mA \cdot cm^{-2}$ with potential window of 0-0.6 V); mesoporous Co_3O_4 microspheres [21] (102 $F \cdot g^{-1}$ at the sweep rate of 3 $mV \cdot s^{-1}$ between the potential range of 0.1-0.6 V) and needle-like Co_3O_4 nanorods [20] (111 $F \cdot g^{-1}$ at the current density of 2.5 $mA \cdot cm^{-1}$ with potential window of 0-0.5 V). The discharge capacitance of Co_3O_4 nano/micro superstructures electrode decreased with the increase in charge-discharge current densities, which was responsible for the internal resistance and polarization of the electrode [34]. As a result, the Co_3O_4 nano/micro superstructures are appropriate for applications in supercapacitors to be used at low current density.

To evaluate the electrochemical capacitance of the Co_3O_4 samples as a function of the heating temperatures, chronopotentiometry were conducted on Co_3O_4 samples with different annealing

temperature. Fig. 6d shows the potential versus time for the electrode made by the annealing temperature of 450, 550 and 650 ℃, respectively. It can be seen that the discharge time decreased with the increase of annealing temperature, which implies the decline of specific capacitance for the Co_3O_4 electrode. Once the oxide phase is formed, further heat-treatment at higher temperature may cause the increase in crystal size, and accordingly a decrease in specific surface area, and also possibly its reactivity for surface chemical process, thereby leading to a decreased capacitance.

The cycling stability for the Co_3O_4 nano/micro superstructures is an important quality require for practical applications, and examined by the continuous charge-discharge measurements over 1000 cycles (the Co_3O_4 sample was obtained at an annealing temperature of 450 ℃). Fig. 6e shows the specific capacitance variation for the Co_3O_4 samples as a function of cycle number at the current density of $1A \cdot g^{-1}$ within a voltage range between 0.00 and 0.35 V in 6 M KOH electrolyte. During the first 130 cycles, the specific capacitance increased from *ca.* 206 to 210 $F \cdot g^{-1}$, resulting from the activation process of the Co_3O_4 electroactive material. Thereafter, it decreases to 204 $F \cdot g^{-1}$ after the subsequent 870 continuous cycles. The lowest specific capacitance after 1000 cycles remains 97% of the maximum capacitance. This demonstrates that the charge-discharge processes do not seem to induce significant structural changes of the Co_3O_4 electrode materials as expected for pseudo-capacitance reactions. The cycling life test suggests that the porous Co_3O_4 nano/micro superstructures electrode has high stability for long-term applications.

4. CONCLUSIONS

In summary, Co_3O_4 nano/micro superstructures assembled by uniform nanoparticles and porous microsheets have been prepared by solid-state thermal decomposition from a cobalt ion-based coordination polymer. The Co_3O_4 nano/micro superstructures have been applied to supercapacitor, it could deliver a specific capacitance of 208 $F \cdot g^{-1}$ at a current density of $1A \cdot g^{-1}$ and offers a lower specific capacitance degradation of *ca.* 3% after 1000 cycles in 6.0 M aqueous KOH solution (vs. SCE). This indicates that the Co_3O_4 nano/micro superstructures can provide simultaneous larger specific capacitance and higher electrochemical stability. The results showed that the Co_3O_4 nano/micro superstructures might have potential applications in supercapacitors. We expected that the preparation strategy of Co_3O_4 nano/micro materials reported here should be viable to extend to other transitional metal oxides systems.

ACKNOWLEDGEMENTS

This work was supported by the National Natural Science Foundation of China under grant No. 20633040, 20873064 and Nanjing University of Aeronautics and Astronautics Research Funding under grant No. NS2010170.

References

1. B.E. Conway, *Electrochemical Supercapacitors, in: Scientific Fundamental and Technological Applications*, Kluwer Academic/Plenum press, New York (1999)

2. L.T. Lam, R. Louey, *J. Power Sources* 158 (2006) 1140
3. M. Winter, R.J. Brodd, *Chem. Rev*. 104 (2004) 4245
4. T.Y. Wei, C.H. Chen, H.C. Chien, S.Y. Lu, C.C. Hu, *Adv. Mater*. 21 (2009) 1
5. B. Liu, H. Shioyama, H.L. Jiang, X.B. Zhang, Q. Xu, *Carbon* 48 (2010) 456
6. H. Jiang, T. Zhao, C.Y. Yan, J. Ma, C.Z. Li, *Nanoscale* 2 (2010) 2195
7. D.C. Wang, W.B. Ni, H. Pang, Q.Y. Lu, Z.J. Huang, J.W. Zhao, *Electrochim. Acta* 55 (2010) 6830
8. Y.G. Guo, J.S. Hu, L.J. Wan, *Adv. Mater*. 20 (2008) 2878
9. C.Z. Yuan, X.G. Zhang, L.H. Su, L.F. Shen, *J. Mater. Chem*. 19 (2009) 5772
10. W. Wei, Z.Z. Yang, *Adv. Mater*. 20 (2008) 2965
11. H.K. Lin, C.B. Wang, H.C. Chiu, S.H. Chien, *Catal. Lett.* 86 (2003) 63
12. D.N. Srivastava, N. Perkas, G.A. Seisenbaeva, Y. Kolty-pin, V.G. Kessler, A. Gedanken, *Ultrason. Sonochem.* 10 (2003) 1
13. K. Ebitani, H.B. Ji, T. Mizugaki, K. Kaneda, *J. Mol. Catal*. A 212 (2004) 161
14. S. Takada, M. Fujii, S. Kohiki, T. Babasaki, H. Deguchi, M. Mitome, M. Oku, *Nano Lett*. 1 (2001) 379
15. E.L. Salabas, A. Rum-plecker, F. Kleitz, F. Radu, F. Schueth, *Nano Lett*. 6 (2006) 2977
16. A.M. Cao, J.S. Hu, H.P. Liang, W.G. Song, L.J. Wan, X.L. He, X.G. Gao, S.H. Xia. *J. Phys. Chem*. B 110 (2006) 15858
17. H.J. Nam, T. Sasaki, N. Koshizaki, *J. Phys. Chem*. B 110 (2006) 23081
18. F.M. Zhan, B.Y. Geng, Y.J. Guo, *Chem. Eur. J*. 15 (2009) 6169
19. G.X. Wang, H. Liu, J. Horvat, B. Wang, S.Z. Qiao, J. Park, H.J. Ahn, *Chem. Eur. J*. 16 (2010) 11020
20. T. Zhu, J.S. Chen, X.W. Lou, *J. Mater. Chem*. 20 (2010) 7015
21. L. Wang, X.H. Liu, X. Wang, X.J. Yang, L.D. Lu. Curr. *Appl. Phys*. 10 (2010) 1422
22. S.L. Xiong, C.Z. Yuan, X.G. Zhang, B.J. Xi, Y.T. Qian, *Chem. Eur. J*. 15 (2009) 5320
23. Y.J. Xiong, Y. Xie, Z.Q. Li, C.Z. Wu, *Chem. Eur. J*. 9 (2003) 1645
24. Z.Q. Li, Y.J. Xiong, Y. Xie, *Nanotechnology* 16 (2005) 2303
25. H.L. Li, M. Eddaoudi, M. O'keeffe, O.M. Yaghi, *Nature* 402 (1999) 276
26. M. Eddaoudi, J. Kim, N. Rosi, D. Vodak, J. Wachter, M. O'keeffe, O.M. Yaghi, *Science* 295 (2002) 469
27. J.F. Arenas, J.I. Marcos, *Spectrochim. Acta* 36A (1980) 1075
28. S.G. Baca, I.G. Filippova, O.A. Gherco, M. Gdaniec, Y.A. Simonov, N.V. Gerbeleu, P. Franz, R. Basler, S. Decurtins, *Inorg. Chim. Acta* 357 (2004) 3419
29. S. Palmas, F. Ferrara, A. Vacca, M. Mascia, A.M. Polcaro, *Electrochim. Acta* 53 (2007) 400
30. C. Xu, B. Li, H. Du, F. Kang, Y. Zeng, *J. Power Sources* 180 (2008) 664
31. V. Subramanian, H. Zhu, R. Vajtai, P.M. Ajayan, B. Wei, *J. Phys. Chem*. B 109 (2005) 20207
32. W. Sugimoto, H. Iwata, Y. Yasunaga, Y. Murakami, Y. Takasu, *Angew. Chem*. 115 (2003) 4226
33. G.Q. Zhang, Y.Q. Zhao, F. Tao, H.L. Li, *J. Power Sources* 161 (2006) 723
34. Y.G. Wang, Y.Y. Xia, *J. Electrochem. Soc*. 153 (2006) A450